Macromolecular Bioscience
www.mbs-journal.de

Ionically Modified Gelatin Hydrogels Maintain Murine Myogenic Cell Viability and Fusion Capacity

*Margherita Burattini, Robrecht Lippens, Nicolas Baleine, Melanie Gerard, Joeri Van Meerssche, Chloë Geeroms, Jérémy Odent, Jean-Marie Raquez, Sandra Van Vlierberghe, and Lieven Thorrez**

For tissue engineering of skeletal muscles, there is a need for biomaterials which do not only allow cell attachment, proliferation, and differentiation, but also support the physiological conditions of the tissue. Next to the chemical nature and structure of the biomaterial, its response to the application of biophysical stimuli, such as mechanical deformation or application of electrical pulses, can impact in vitro tissue culture. In this study, gelatin methacryloyl (GelMA) is modified with hydrophilic 2-acryloxyethyltrimethylammonium chloride (AETA) and 3-sulfopropyl acrylate potassium (SPA) ionic comonomers to obtain a piezoionic hydrogel. Rheology, mass swelling, gel fraction, and mechanical characteristics are determined. The piezoionic properties of the SPA and AETA-modified GelMA are confirmed by a significant increase in ionic conductivity and an electrical response as a function of mechanical stress. Murine myoblasts display a viability of >95% after 1 week on the piezoionic hydrogels, confirming their biocompatibility. The GelMA modifications do not influence the fusion capacity of the seeded myoblasts or myotube width after myotube formation. These results describe a novel functionalization providing new possibilities to exploit piezo-effects in the tissue engineering field.

1. Introduction

About 40% of the human body mass consists of skeletal muscle. Upon injury, the skeletal muscle tissue has the capacity to regenerate itself using tissue-resident stem cells, the satellite cells. However, when there is a substantial loss in muscle tissue, the remaining tissue is unable to restore the defect fully. This volumetric muscle loss (VML) results in the development of scar tissue and has a negative impact on the patients' morbidity and life quality. To eliminate the need of an autologous muscle transfer as a main resolution to the VML,[1–4] the engineering of muscles as clinical substitutes is therefore an important aim of the field.[5] As a consequence, off-the-shelf biomimetic scaffolds for skeletal muscle regeneration need to be developed.[1] These scaffolds need to support the cells' proliferation and differentiation to produce a construct that mimics the physiology of skeletal muscle as close as possible. For this, different procedures to engineer 3D in vivo-like structures or bioartificial muscles (BAMs) were already described.[6–10] The most used materials as a biomimetic scaffold for BAMs are fibrin and collagen.[7,8,10–12] Gelatin, as a collagen derivate, is considered an interesting material for several reasons. It is a natural biodegradable polymer with extensive tunability thanks to (photo-)cross-linkable functionalities.[13–15] Moreover, it is cheap and easily manipulable.[16] As a consequence, cross-linkable gelatins have become a benchmark in many fields of bio-fabrication and tissue engineering.[15] One of the most used gelatin-based hydrogels is the gelatin methacryloyl (GelMA). GelMA hydrogels closely resemble some essential properties of native extracellular matrix (ECM), such as the presence of cell-attaching and matrix responsive peptide motifs (RGD), which allow cells to attach, proliferate, and spread in the scaffolds.[14,17]

Besides the supportive properties, other hydrogel characteristics might further promote the formation of engineered tissue. For example, a typical property of skeletal muscle is the electrical activity occurring in the tissue.[18] Therefore, the use of an electroconductive hydrogel as a scaffold for muscle tissue engineering could help to provide electrical cues to the cells, contributing to the alignment, proliferation, and differentiation of

M. Burattini, M. Gerard, L. Thorrez
Tissue Engineering Lab, Dep. Development and Regeneration
KU Leuven Kulak
Kortrijk 8500, Belgium
E-mail: margherita.burattini@univr.it; lieven.thorrez@kuleuven.be
M. Burattini
Dep. Of Surgical Sciences, Dentistry and Maternity
University of Verona
Verona 37129, Italy
R. Lippens, J. Van Meerssche, C. Geeroms, S. Van Vlierberghe
Polymer Chemistry & Biomaterials Group, Center of Macromolecular Chemistry (CMaC), Dep. Of Organic and Macromolecular Chemistry
Ghent University (UGent)
Ghent 9000, Belgium
N. Baleine, J. Odent, J.-M. Raquez
Laboratory of Polymeric and Composite Materials (LPCM), Center of Innovation and Research in Materials and Polymers (CIRMAP)
University of Mons (UMONS)
Place du Parc 20, Mons 7000, Belgium

The ORCID identification number(s) for the author(s) of this article can be found under https://doi.org/10.1002/mabi.202300019

DOI: 10.1002/mabi.202300019

muscle cells.[19] Hydrogels with conductive properties can be synthesized by conjugating conductive polymers or by incorporating conductive nanomaterials into the backbone of polymer networks.[20] An attractive way of providing electric current to the engineered muscle without using an external electric power source involves the use of electromechanical materials.[21,22] These materials produce an electric current induced by a mechanical deformation. The electromechanical transduction includes piezoresistive, piezoelectric, piezoionic, and capacitive mechanisms.[23] Among them, typical piezoionic materials consist of a polyelectrolyte hydrogel containing fixed macro-ions and mobile counterions. Under indentation, the mechanical deformation entrains the mobile counterions to flow from the point of compression, generating a charge imbalance within the polyelectrolyte hydrogel and leading to a voltage induction. Some biological polymers, such as collagen, fibrin, and cellulose, already exhibit mild electromechanical characteristics.[24–27] These can be further enhanced by the incorporation of mobile ions in the scaffold material. Nowadays, an increasing amount of materials with improved electrical and mechanical properties find their application in tissue regeneration.[28] Specifically, Odent et al. developed new self-powered piezoionic sensors, which utilize touch-induced ionic charge separation in 3D-printed ionically modified polyacrylamide hydrogels.[29] In this work, cationic 2-acryloxyethyltrimethylammonium chloride (AETA) and anionic 3-sulfopropyl acrylate potassium (SPA), whose charges are balanced by mobile Cl^- anions and K^+ cations respectively, are chemically incorporated in photo-crosslinkable hydrogels based on GelMA.[28–33] This GelMA modification involves the generation of an output voltage induced by the separation of ions of different mobilities, stimulated by a mechanical load applied to the material.

2. Results and Discussion

In order to produce piezoionic materials, GelMA was combined with the ionic SPA and AETA monomers, which were chemically incorporated as previously described.[21,30] The starting material for GelMA was gelatin type B (Gel-B), on which the photo-crosslinkable methacrylamide moieties were introduced to the gelatin side chains. An o-phthaldialdehyde (OPA) assay demonstrated a degree of substitution (DS) of 95% for GelMA. This was then used for all characterization tests at a concentration of 10% w/v. The physico-chemical properties of GelMA 30% SPA and GelMA 30% AETA, with charges balanced by K^+ cations and Cl^- anions, respectively, were compared to the control with no ionic monomers, termed GelMA 0% ion.

The cross-linking efficiency of Gel-MA 0% ion, Gel-MA 30% SPA, and Gel-MA 30% AETA equaled 80%, 90%, and 80%, respectively (HR-MAS ^{1}H NMR spectra of Gel-MA 0% ion shown in **Figure 1**; see Figures S1 and S2, Supporting Information for GelMA 30% SPA and GelMA 30% AETA). The similar cross-linking efficiencies of the samples indicated that the incorporated SPA and AETA monomers did not interfere with the GelMA cross-linking reaction. The obtained cross-linking efficiency of Gel-MA 0% ion was slightly higher compared with previous literature reports referring to a cross-linking efficiency of ≈70% for 10% w/v Gel-MA hydrogels based on a degree of substitution of 95%.[31]

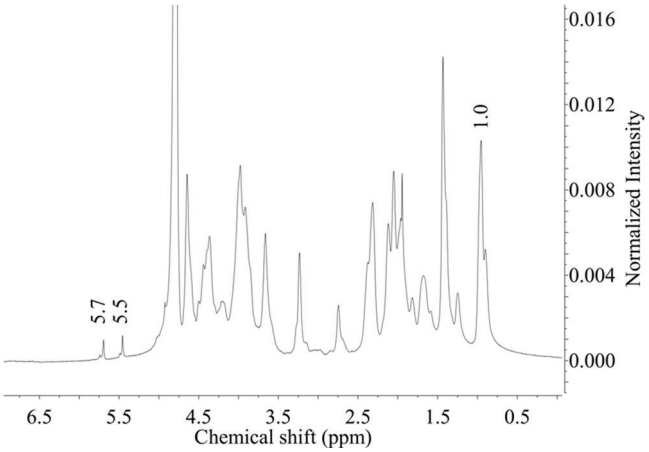

Figure 1. HR-MAS ^{1}H NMR spectrum of crosslinked Gel-MA (DS 95%, 10% w/v) with the characteristic methacrylamide signals at 5.5 and 5.7 ppm and the reference signal at 1.0 ppm corresponding to the $-CH_3$ groups present in valine, leucine, and isoleucine.

The photo-crosslinking kinetics of GelMA 30% SPA and GelMA 30% AETA were assessed with in situ photo-rheology (**Figure 2**a). The results demonstrate that during the physical gelation at 5 °C during the first 15 min, the three hydrogels showed a similar increase in storage modulus. However, the addition of SPA and AETA led to faster cross-linking kinetics upon UV-light irradiation (Figure 2b). Additionally, the mechanical properties of the three types of equilibrium swollen GelMA hydrogel films in aqueous solution, were determined with rheology (Figure 2c). The storage moduli were respectively 31.6 ± 3.5, 26.4 ± 9.9, and 48.2 ± 3.7 kPa for GelMA 0% ion, GelMA 30% SPA, and GelMA 30% AETA. A significant difference was detected between the storage moduli of GelMA 0% ion and GelMA 30% AETA ($p < 0.05$).

The probability of a hydrogel to leach potentially harmful cytotoxic substances was assessed by measuring the gel fraction (Figure 2d). In all conditions, a high gel fraction of ≈100% was detected, indicating no significant leaching of components. More specifically, the following gel fractions were measured for GelMA 0% ion (99.6 ± 1.6%), GelMA 30% SPA (94.5 ± 3.1%), and GelMA 30% AETA (97.0 ± 4.6%). There was a significant difference detected between GelMA 30% SPA and GelMA 0% ion ($p < 0.05$), while GelMA 30% AETA was not significantly different. In Figure 2e, the mass swelling is depicted, indicating the ability of the hydrogel to swell in aqueous medium without dissolving. The measured mass swelling ratios were 16.2 ± 1.5, 18.4 ± 1.4, and 18.6 ± 0.9 for GelMA 0% ion, GelMA 30% SPA, and GelMA 30% AETA, respectively. A significant increase in mass swelling ratios was observed for both the SPA and AETA modified GelMA samples compared to GelMA 0% ion. Furthermore, the biodegradability of the cross-linked hydrogels was determined with an in vitro enzymatic degradation assay (Figure 2f). All GelMA hydrogel films (0% ion, 30% SPA, and 30% AETA) were enzymatically degradable with degradation times of 243.9, 281.7, and 259.2 min for GelMA 0% ion, GelMA 30% SPA, and GelMA 30% AETA, respectively. No significant difference was observed between the aforementioned conditions ($p > 0.05$).

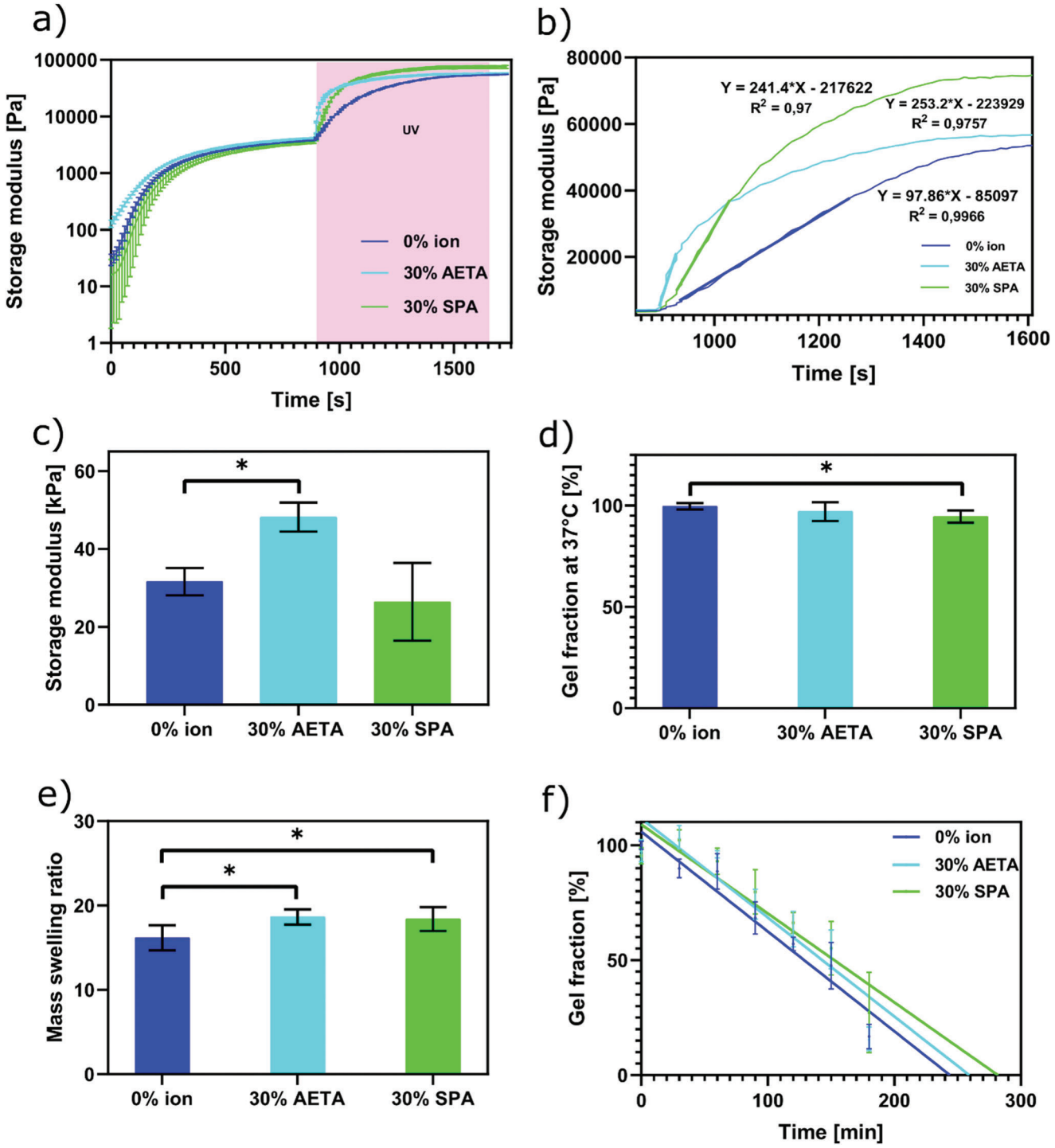

Figure 2. Physico-chemical characterization of GelMA and ionically modified GelMA. a) In situ rheology on 10% w/v solution of GelMA (0% ion, 30% SPA, and 30% AETA) in the presence of 2 mol.% Li-TPO-L. The storage modulus increases during the first 900 s when physical gelation at 5 °C occurs. b) Cross-linking upon UV-A light exposure (indicated by the pink background in panel a). c) Comparison of the storage moduli (G') after rheology on equilibrium swollen hydrogel films. d) Gel fraction comparison between the three GelMA conditions. e) Mass swelling ratio comparison between the GelMA conditions. A higher mass swelling ratio in the ionic modifications compared to the control without ions can be seen. f) In vitro enzymatic degradation comparison between the different GelMA experimental specimen. Statistical analysis: Kruskal–Wallis test and Dunn's correction with $^{*}p < 0.5$.

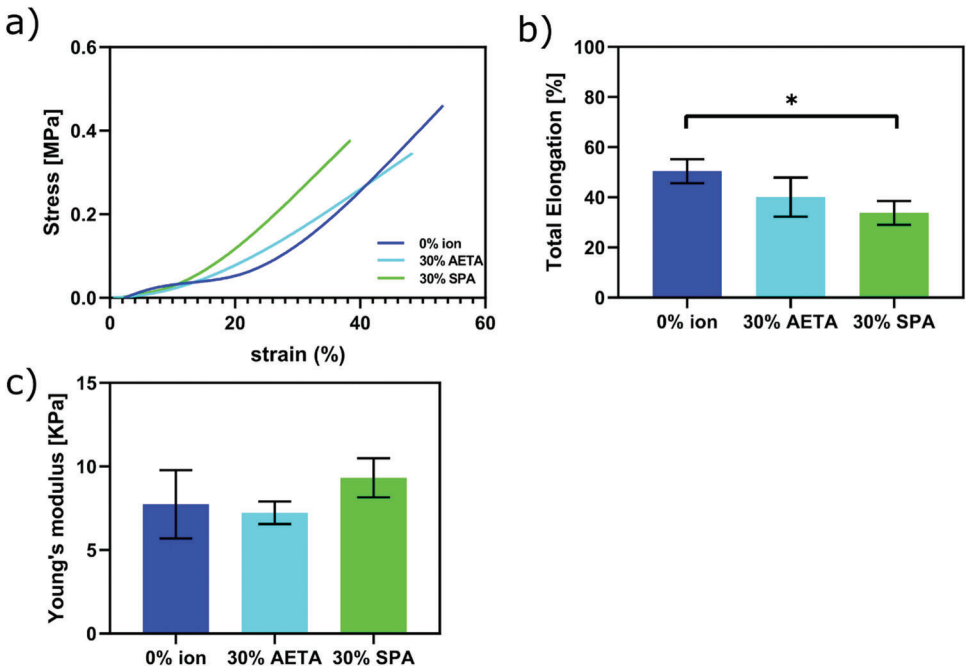

Figure 3. Mechanical characterization of GelMA and ionically modified GelMA. a) Stress–strain curves of GelMA loops (GelMA 0% ion, 30% SPA, and 30% AETA). b) Total elongation (%) before fracture of the GelMA hydrogel loops, which was significantly reduced in the GelMA with SPA functionalization. c) Young's modulus (kPa) of the GelMA hydrogel loops. Statistical analysis: Kruskal–Wallis test with Dunn's correction with $^{*}p < 0.05$.

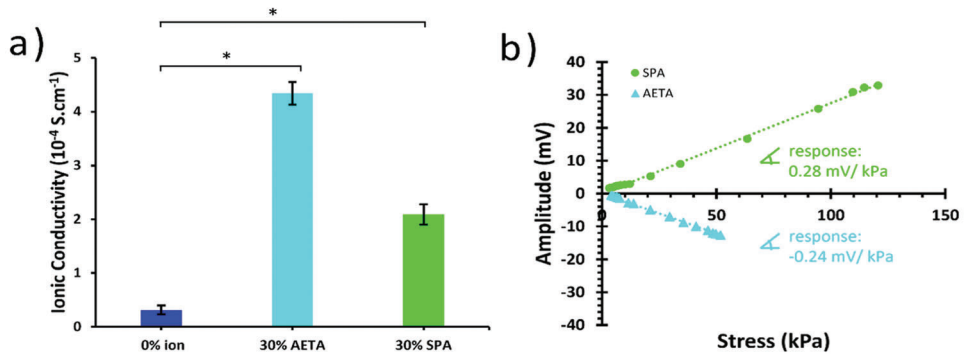

Figure 4. Electromechanical characterization of GelMA and ionically modified GelMA. a) ionic conductivity of GelMA (GelMA 0% ion, 30% SPA, and 30% AETA). b) electromechanical response as a function of stress for GelMA 30% SPA and GelMA 30% AETA gels. Statistical analysis: Kruskal–Wallis test with Dunn's correction with $^{*}p < 0.05$.

In addition, tensile tests were conducted to determine the total elongation (%) and the Young's modulus (kPa) of the hydrogel loops (**Figure 3**a). The % elongation before fracture was 50.4 ± 4.8%, 33.8 ± 4.7%, and 40.1 ± 7.8% for GelMA 0% ion, GelMA 30% SPA, and GelMA 30% AETA, respectively (Figure 3b). A significant difference was detected between the total elongation of GelMA 30% SPA and GelMA 0% ion ($p < 0.05$). The Young's moduli were 7.7 ± 2.0, 9.3 ± 1.2, and 7.2 ± 0.7 kPa for GelMA 0% ion, GelMA 30% SPA, and GelMA 30% AETA, respectively, which was not significantly different between the three conditions ($p > 0.05$) (Figure 3c).

The ionic conductivity was further assessed by impedance spectroscopy and estimated at $3.14\times10^{-5} \pm 0.83\times10^{-5}$, $4.34\times10^{-4} \pm 0.21\times10^{-4}$, and $2.09\times10^{-4} \pm 0.19\times10^{-4}$ S cm^{-1} for GelMA 0% ion, GelMA 30% SPA, and GelMA 30% AETA, respectively (**Figure 4**a). A significant increase in ionic conductivity was observed for the SPA and the AETA-modified GelMA samples compared to the GelMA 0% ion. The electromechanical response was assessed using an open circuit voltage measurement of the potential (Figure 4b). Under compressive strains using a cylindrical indenter of outer diameter 4 mm, an initial viscoelastic deformation entrains the mobile counterions to flow from the point of compression, generating a charge imbalance within the ionically modified GelMA hydrogel which in turn leads to an output voltage. Overall, a preferential displacement of the cations over anions results in a positive voltage reading, and vice versa. As expected, no response as a function of the compressive strain was observed for GelMA 0% ion while −0.24

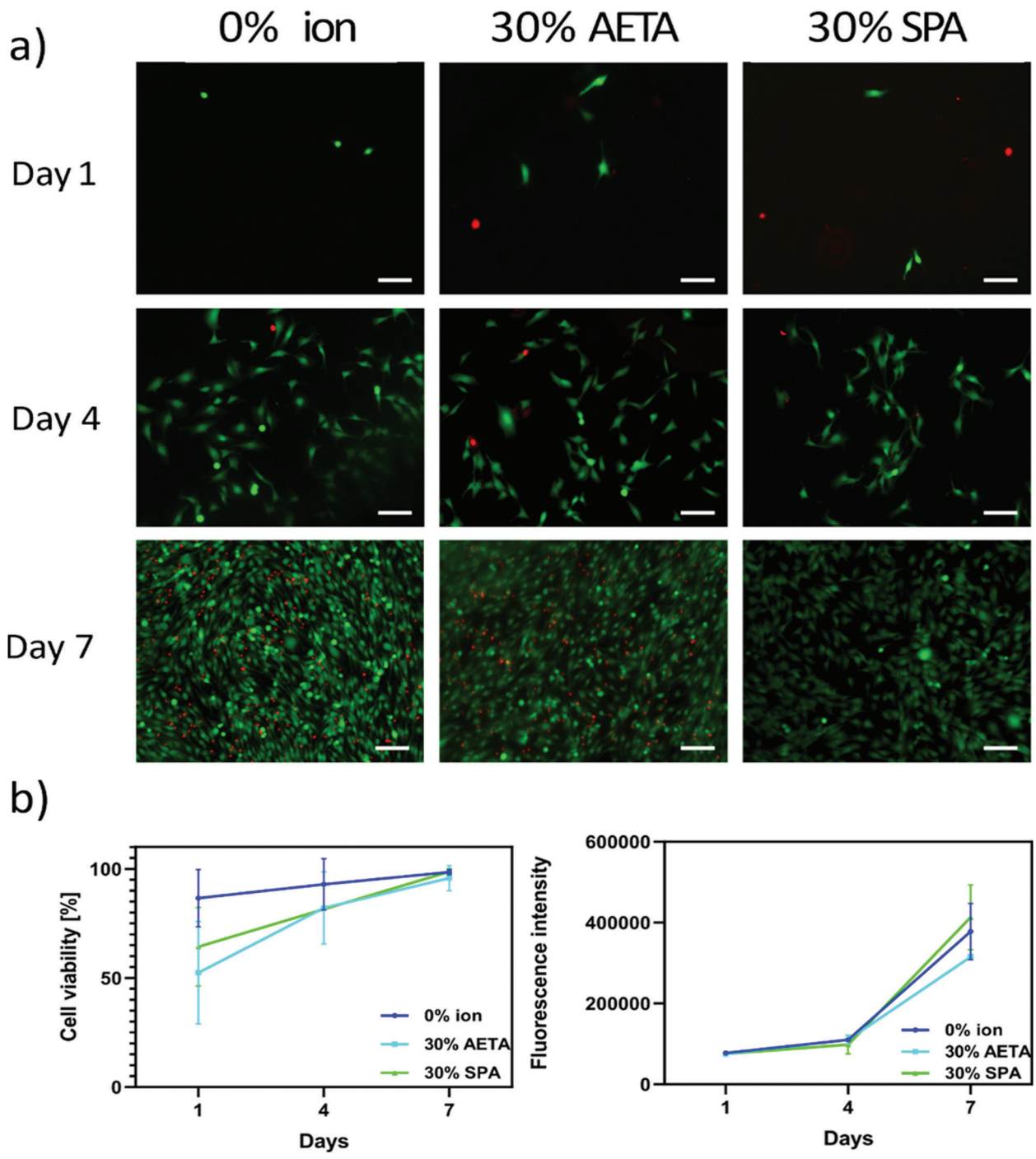

Figure 5. Live/dead viability assay on cross-linked GelMA DS95 10% w/v (0% ion, 30% AETA, 30% SPA). The hydrogel films were seeded with 5000 *C2C12* cells. Scalebar: 50 µm. a) Live/dead images were taken on days 1, 4, and 7. b) Quantification of the cell viability (left panel). A metabolic (Alamar Blue) assay was performed on seeded *C2C12* cells on GelMA DS95 10% w/v (0% ion, 30% AETA, and 30% SPA) hydrogel films (right panel).

and +0.28 mV kPa^{-1} were recorded for GelMA 30% AETA and GelMA 30% SPA, respectively.

The biocompatibility of SPA and AETA GelMA films (DS95, 10% w/v) films was assessed with the additional anion SPA and cation AETA. Using the Calcein-AM/PI staining, the cell viability of the seeded *C2C12* cells was determined on days 1, 3, and 7 (**Figure 5**a). After 24 h of cell seeding, the cell viability was 88.3 ± 13.2%, 52.4 ± 23.4%, and 64.3 ± 18.0% for GelMA 0%, GelMA 30% AETA, and GelMA 30% SPA, respectively. No significant difference was detected for GelMA 30% AETA and GelMA 30% SPA in comparison to GelMA 0% ion ($p > 0.05$). However, note that there was a high variability, especially a higher initial

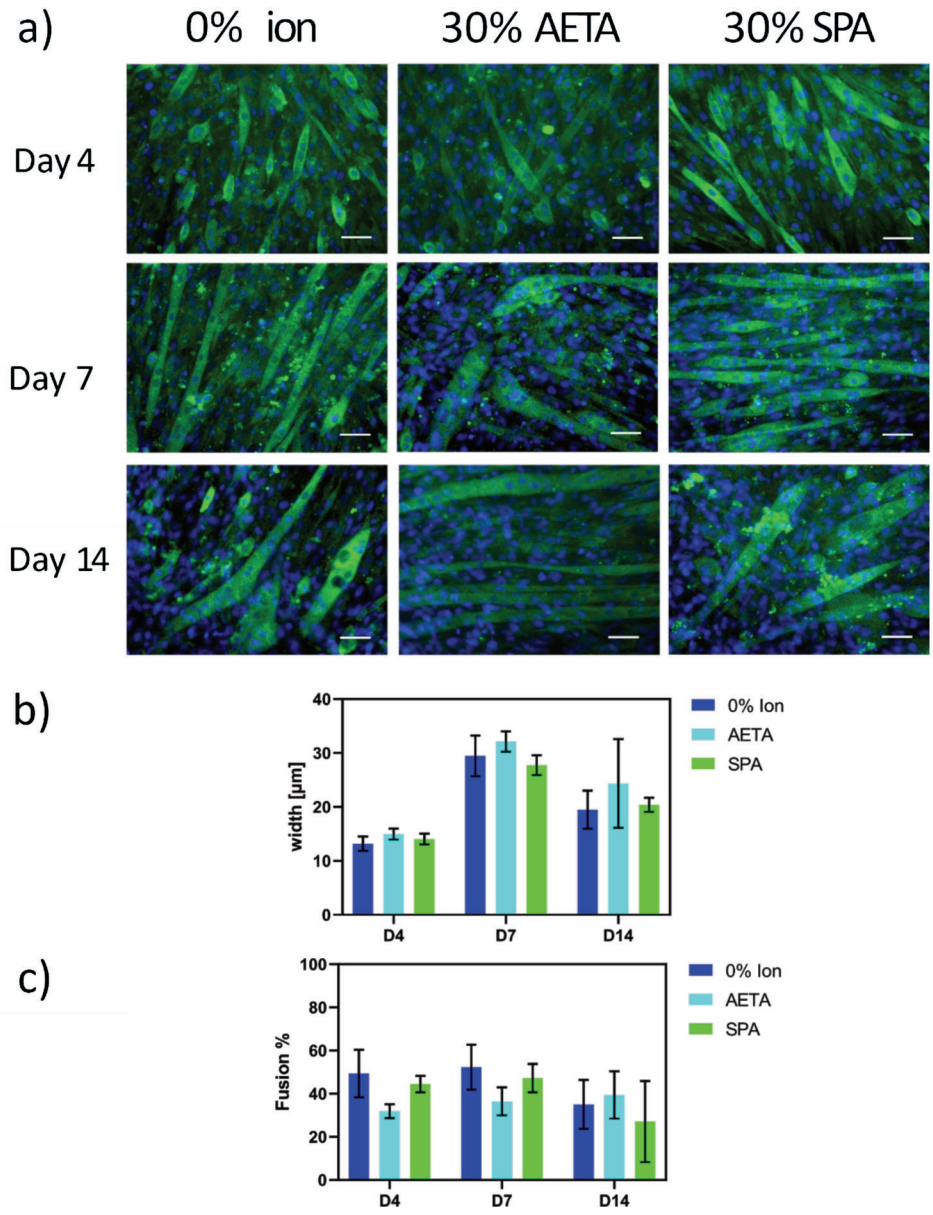

Figure 6. Fusion capacity followed up to D14 of culture over the three different materials. a) Representative Tropomyosin/DAPI fluorescent images of myotubes formed from differentiated C2C12 myoblasts seeded on GelMA with respectively 0% ion, 30% SPA, and 30% AETA on days 4, 7, and 14. Blue: DAPI, green: tropomyosin. Scalebar: 50 µm. b) Fiber width calculated from the immunofluorescence images. c) Fusion indices calculated from the immunofluorescence images. Statistical analysis: Kruskal–Wallis test with Dunn's correction.

viability for GelMA 0% ion, due to the small sample size, leading to no statistical difference at day 1. Over time, the viability in the AETA and SPA group increased (Figure 5b). At day 4, the cell viability was raised to 92.9 ± 11.1%, 82.1 ± 16.5%, and 81.5% for GelMA 0% ion, GelMA 30% AETA, and GelMA 30% SPA, respectively. Ultimately, 1 week after cell seeding, the *C2C12* cells had reached a cell viability of 98.5 ± 1.2%, 95.7 ± 5.7%, and 98.7 ± 1.4% for GelMA 0% ion, GelMA 30% AETA, and GelMA 30% SPA, respectively. At days 4 and 7, no significant difference in cell viability was detected between the three experimental conditions ($p > 0.05$). Furthermore, an Alamar Blue Assay, which can detect changes in metabolic activity of the cells, showed no significant difference for the metabolic activity of the *C2C12* cells between the three GelMA conditions ($p > 0.05$) (Figure 5b, right panel).

To verify whether the hydrogel compositions affected the differentiation potential of the *C2C12* cells to fuse and form myotubes, the fusion index and myotube width was calculated. The immunofluorescence staining for tropomyosin was performed at days 4, 7, and 14 on the 4% PFA-fixed samples (**Figure 6**). The experimental days have to be intended as days in culture in differentiation medium. No differences in fusion capacity nor myotube width were observed between the different GelMA hydrogels (Figure 6b).

3. Conclusion

In the field of skeletal muscle tissue engineering, the addition of mechanical and electrical stimuli to the scaffolds plays a pivotal role in the function, proliferation, and differentiation of the skeletal muscle cells.[32] Additionally, electrical cues fulfill an essential role in the morphology and migration of the cells.[33] Therefore, constructing a hydrogel material with electroconductive properties is a very promising route in the field of skeletal muscle tissue engineering. Electroconductive GelMA hydrogels have previously been developed by Wu et al.[34] by integrating poly(aniline) (PANi) within GelMA. These formed hydrogels demonstrate similar mechanical and swelling properties to the benchmark GelMA, but with superior electrical properties.[34] Moreover, Sawyer et al.[35] developed GelMA-PANi bio-inks with encapsulated osteogenic cells, demonstrating similar cell viability compared to GelMA.[35] In the present work, the anionic SPA and the cationic AETA, with charge balanced by Cl^- anions and K^+ cations, respectively, were chemically incorporated to develop a piezoionic GelMA hydrogel. The resulting ionically modified GelMA exhibited high conductivity compared to 0% ion GelMA and generated an output voltage in response to mechanical deformation. The polarity of output voltages is herein consistent with the movement of the mobile counterions away from the indented region. As a consequence, positive and negative voltages respectively arise from anionic SPA- and cationic AETA-modified GelMA. Interestingly, these intrinsic electromechanical properties of ionically modified GelMA offer the possibility to induce electromechanical cues caused by the movement of cells, or on the contrary, allowing the electromechanical stimulation of cells.

The physico-chemical properties of GelMA hydrogel films with incorporated anionic SPA or cationic AETA functionalities were determined. A high gel fraction was obtained for all the GelMA conditions (0% ion – 30% SPA – 30% AETA), indicating an efficient crosslinking of the hydrogel films and minimal leaching of components. The gel fraction results of GelMA without ions were in line with previously reported data by Van Nieuwenhove et al.[36] and demonstrated the efficient UV-photo-crosslinking of the hydrogels.[13,15] This can be explained by the high DS of 95% and the use of 10% w/v, resulting in a high probability for the functionalities of GelMA to efficiently react. Due to the high amount of reacted functionalities as demonstrated by HR-MAS NMR spectroscopy, efficient crosslinking occurred and a stable GelMA network was formed.

Furthermore, the addition of the SPA anion and the AETA cation led to an increase in the mass swelling ratio of the GelMA hydrogel films. This increase can be explained by the increased charge density in the GelMA hydrogel films, due to the addition of positively charged AETA or negatively charged SPA.[37] These additional charges could create an osmotic effect and therefore attract more water.[38–40]

The photo-crosslinking of GelMA was also influenced by the addition of these ionic functionalities to the GelMA network, as there was a significant increase detected in the cross-linking rate. This can be explained by the higher concentration of unsaturated bonds available due to the addition of AETA or SPA to GelMA.[41] Both ionic modifications have acrylate groups that can crosslink with the functional methacrylamide groups of GelMA upon exposure to UV-light. The cross-linking rate of SPA/AETA-modified GelMA when exposed to UV-light was increased compared to the regular GelMA, thanks to a higher number of cross-linkable functionalities of the former.[43] Furthermore, the storage modulus of the equilibrium swollen hydrogel films was also assessed, with the storage modulus of GelMA 0% ion being in accordance with previously reported data by Van Hoorick et al.[42] The significantly higher storage modulus of GelMA AETA can again be explained by the higher concentration of acrylate functionalities. The effect of the increased amount of unsaturated bonds on the storage modulus upon the addition of cationic AETA is comparable to the effect of a higher DS or %w/v.[42] Upon using a higher DS or %w/v, the amount of double bounds is higher, resulting in an increase in storage modulus after UV-light exposure.[43] In order to gain more insight in the differences in the cross-linking efficiency of SPA/AETA-modified GelMA versus the unmodified GelMA, HR-MAS NMR spectroscopy was performed. SPA and AETA had no major impact on the cross-linking efficiency.[44]

Next, GelMA 0% ion, 30% SPA, 30% AETA hydrogel loops were subjected to tensile tests. The Young's modulus of the loops was determined from the linear part of the stress–strain curves and were in line with previously reported results by Rajabi et al.[45] No significant differences were observed between the Young's moduli of the three samples. Moreover, a Young's modulus in the range of a few kPa is an ideal environment for myotube differentiation.[15,34] Nonetheless, the material studied offers great flexibility and multiple solutions to modify the stiffness making it an ideal substrate for culturing muscle cells.[15] Furthermore, the ionic modifications caused an increase in the swelling properties, which may lead to higher cell infiltration, higher diffusion as well as higher surface to volume ratio.[13,46] The similar physico-chemical properties and cytocompatibility when AETA and SPA were chemically incorporated in comparison to the GelMA without ions indicate that the introduced modifications constitute a usable hydrogel. Conductive measurements have been performed showing that the addition of AETA or SPA enhances the conductivity of the hydrogel by a factor 10.[35] Therefore, GelMA with incorporated AETA cations or SPA anions could be used as a conductive scaffold material to test cytotoxicity and possible positive effects for enhancing culture conditions. This result reports a new favorable niche for the generation of small currents in the presence of mechanical pressure and making the cues as physiological as possible. The duality given by the piezoionicity would allow researchers to study multiple culture conditions.

In vitro cell tests on *C2C12* cells were conducted to determine the possible cytotoxicity of the anionic SPA and cationic AETA functionalities. For the seeded *C2C12* cells, a live/dead staining was performed on days 1, 4, and 7. After 1 week, *C2C12* cells seeded on GelMA hydrogel films (0% ion, 30% SPA, and 30% AETA), showed no statistical difference in viability, for all the experimental conditions. High cell viability (>95%) of the seeded *C2C12* cells on GelMA with a DS of 95% and at 10% w/v agreed with previously reported results by Chen et al.[47] where ≈92% of viable cells was reported after 5 days. Although at the first time point (day 1) measured, there was a large variability in the cell viability, the later time points (days 4 and 7) showed that the addition of additional ions to the GelMA hydrogel did not affect cell proliferation. Additionally, a metabolic assay, which quantifies number and metabolic activity of the cells, was

performed on days 1, 4, and 7 of culture. The data demonstrate that after 4 days the proliferation increased, but no significant difference was detected between the three conditions. The former is in line with earlier reported results from Kim et al.[48] In these experiments, the cells were not seeded onto GelMA film but encapsulated instead.[48] Overall, we can conclude that the SPA or AETA functionalization was not cytotoxic for the *C2C12* cells.[15,27,36,46] Lastly, we performed an immunofluorescence staining to further study any differences in the differentiation of the cells on the three materials. As in the proliferation stage, the differentiation phase of the cells occurred similarly in the AETA and SPA-modified GelMA as in the unmodified GelMA. Future studies may be geared toward testing the possible enhancement on myotube development when applying a mechanical stimulation protocol and conversely, an electrical stimulation protocol, to fully use the ability of these piezoionic materials. In conclusion, these findings may help to provide to researchers an off-the-shelf scaffold with a defined and tunable property to better resemble the muscle physiological condition.

4. Experimental Section

Modification of Gelatin: For reaching the desired modification of gelatin, the protocol described earlier by Van den Bulcke et al.[30] was used. Briefly, gelatin type B (Gel-B, 38.5 mmol amines per 100 g) was dissolved in a phosphate buffer (pH 7.8) at 40 °C while stirring. The reaction was initiated by the addition of methacrylic anhydride in 2.5 equivalents (eq), relative to the number of primary amines of Gel-B, to the solution. After stirring the solution vigorously for 1 h, the solution was diluted (1:2) with Milli-Q water and was dialyzed (Spectrapor MWCO 12 000–14 000 Da) for 24 h at 40 °C. After completion of the dialysis, the pH of the solution was adjusted to 7.4 using NaOH (2 M). Finally, the solution was frozen (−20 °C) and lyophilized, in order to obtain dry GelMA. The degree of substitution (DS) was confirmed with the o-phthaldialdehyde (OPA) assay, as described by Tytgat et al.[13] The DS was measured by the absorbance at 335 nm (37 °C) and R^2 was calculated.

Crosslinking: First, a GelMA 10% w/v solution was made by dissolving GelMA in Milli-Q together with 2% Lithium phenyl-2,4,6-trimethylbenzoylphosphinate (Li-TPO-L) photo-initiator (relative to the amount of methacrylamide present, see section 2.1) (Sigma–Aldrich, 900889-5G). GelMA modifications were adopted by blending 30 mol.% of 3-sulfopropyl acrylate potassium (SPA) or [2-(acryloyloxy)ethyl]trimethylammonium chloride (AETA) with the GelMA 10% w/v solution. After dissolving the solutions at a temperature of 40 °C, the mixtures were poured between two glass plates that were separated by a 1 mm silicone spacer. Next, the glass plates were stored in the dark at 4 °C for 20 min to allow physical crosslinking. Then, the GelMA hydrogels were chemically crosslinked by exposure to UV-A light (365 nm, 4 mW cm^{-2}, 20 min). Finally, films were made out of the hydrogel with appropriate punchers to assess the physico-chemical and biocompatibility properties of the hydrogels.

Physico-Chemical Hydrogel Characterization: *Determination of Hydrogel Storage Modulus*: The mechanical properties and photo-crosslinking kinetics were determined using a rheometer (Physica MCR-301, Anton Paar, Sint-Martens-Latem, Belgium). The storage modulus was measured during dynamic oscillation exploiting a parallel plate set-up. Photo-crosslinking kinetics were determined by in situ rheology, by placing a solution containing 2 mol.% Li-TPO-L photoinitiator between the parallel plates of the rheometer in order to evaluate the effect on the storage modulus when exposed to UV-light. Next, the gap between the plates was set to 0.35 mm. Dehydration of the solution was avoided by applying middle viscosity silicone grease on the edges of the plates. During the first 900 s, the temperature of the plates was set at 5 °C to induce physical gelation, while an oscillation frequency of 1 Hz, a strain of 0.1%, and a normal force of 1 N were applied on the forming hydrogel. After physical gelation, the solution was exposed to UV-A light (EXFO Novacure 2000 UV light source at 365 nm using a 3500 mW cm^{-2} intensity) for 10 min at 5 °C, to determine the storage modulus of the cross-linked GelMA.

Gel Fraction Determination: The gel fraction of circular hydrogel films (8 mm diameter, 6 films) was determined. First, the cross-linked films were punched out and lyophilized. After freeze-drying, the initial dry mass (W_{d0}) of the samples was weighed. Next, the discs were incubated and swollen overnight in double distilled water at 37 °C. Subsequently, the samples were lyophilized again and weighed to determine the mass of the samples after incubation (W_{de}). The gel fraction was calculated by comparing the final dry mass to the initial dry mass, as reported in Equation (1).

$$Gel\ fraction\ \ (\%) = \frac{W_{de}}{W_{d0}} x\ 100\ \ (\%) \tag{1}$$

The mass swelling ratio of hydrogel films (8 mm diameter, 6 films), punched out from equilibrium swollen sheets (overnight at 37 °C, in double distilled water), was determined. The swollen mass (M_s) of the films was determined after removal of the excess of water. Next, the samples were lyophilized in order to determine the dry mass (M_d). Finally, the swelling ratio was calculated by comparing the swelling mass to the dry mass (Equation 2):

$$Mass\ swelling\ ratio\ = \frac{M_s}{M_d} \tag{2}$$

Enzymatic Degradation of Hydrogels: The enzymatic degradation assay was conducted on lyophilized hydrogel films (8 mm diameter, $n = 4$ for each timepoint), which were weighted first in order to determine the initial dry mass. Consequently, the samples were incubated in Tris-HCl buffer (0.1 M, pH 7.4), containing 0.005% w/v NaN_3 and $CaCl_2$ (5 mM), at 37 °C for 1 h. Then, collagenase (100 collagen degrading units (CDU)/mL buffer), dissolved in Tris-HCl buffer, was added to the samples.[49] At the predetermined timepoints, the enzymatic degradation was inhibited by the addition of EDTA solution (0.25 mM). After blocking the enzymatic degradation, the samples were cooled in ice. The samples were washed three times in Tris-HCl buffer, followed by washing three times in double distilled water. Next, the samples were freeze-dried and the final dry mass was determined. Using the initial dry mass and the final dry mass, the gel fraction of the samples at each time point could be determined.

Tensile Testing: Tensile testing was performed on photo-crosslinked hydrogel loops swollen to equilibrium with Hounsfield Test Equipment Ltd (Horizon software). The hydrogel loops had a dimension of 28 mm × 3 mm × 1 mm (diameter of 1 mm) and were put around two clamps, which allowed stretching of the hydrogel. The tensile properties of the hydrogel loops were determined with a load cell of 25 N. After placing the hydrogel loop on the two clamps, the loop was subjected to increasing stress and strain at a speed of 5 mm min^{-1} until fracture. The measurements started when the loop was submitted to a force above the threshold 0.05 N. Tensile testing was performed on the hydrogel loops to determine the total elongation and the Young's modulus of the material.

Determination of Cross-Linking Efficiency: High Resolution – Magic Angle Spinning ^{1}H-NMR spectroscopy (HR-MAS NMR) was used to analyze the cross-linking efficiency of GelMA. All measurements were conducted on a Avance II 700 spectrometer (Bruker, 700.12 MHz) with an equipped HR-MAS probe (1H, 13C, 199Sn and a gradient channel). All samples were rotated with a 6 kHz spinning rate. The cross-linked GelMA hydrogels were divided into small pieces, which were introduced with 50 µL D_2O into a 4 mm MAS rotor. After allowing the hydrogel sample to swell, the sample was homogenized by manually stirring the rotor. The cross-linking efficiency (CE) was determined by using Equation (3), as reported earlier by Van Hoorick et al.[42]

$$CE\ \ (\%) = \left[\frac{\frac{I_{5.5ppm} + I_{5.7ppm}}{2 * 0.0385\ \frac{mol}{100g}}}{\frac{I_{1.0ppm}}{0.3836\ \frac{mol}{100g}}} \right] * 100 \tag{3}$$

Cell Culture: For cytotoxicity studies, the murine *C2C12* myoblast cell line was selected. Cells with passage numbers below 20 were used to assure adequate proliferation and differentiation ability. *C2C12* were cultured in growth medium (high glucose DMEM, Gibco, ThermoFisher, #11965092) supplemented with 10% FBS (Biowest) and 1% penicillin/streptomycin solution (P/S, ThermoFisher, 10 000U/mL)). The cells were harvested once reaching 80% confluency and seeded on round GelMA films (10 mm diameter) placed in 24-well plates. Cell seeding density was 10 000 cells per well for proliferation studies and 50 000 cells per well for differentiation assessment. Within 2 days after seeding, in which the cells were cultured in growth medium, the medium was switched to a differentiation medium (high glucose DMEM, 2% horse serum (ThermoFisher) and 1% P/S) for 4, 7, or 14 days to allow the myoblasts to fuse and differentiate into myofibers.

Viability and Metabolic Assays: Calcein acetoxymethyl ester (Calcein-AM)/ propidium iodide (PI) staining was used to assess the live/dead ratio of the seeded C2C12 cells on the GelMA films[50] The live/dead ratio was quantified to assess the cytocompatibility of the GelMA constructs. A solution containing PI and Calcein-AM (both at 0.0002% (v/v) in PBS, Gibco) was added to the hydrogels in the 24-well plate and incubated (10 min, room temperature, shielded from light). Fluorescence microscopy (AxioVert A1, Zeiss) was used to visualize the living and dead cells. Calcein-AM binds to living cells and was visualized with a green fluorescent protein (GFP) filter, while PI visualizes the dead cells and was detected with a Texas Red (TxRed) filter. The live/dead ratio was quantified using ImageJ software, which enables counting of both the living and dead cells. The green (living cells) and red channel (dead cells) were split, and the cells were respectively quantified with the multi-point counting built-in ImageJ function. Live/dead analysis was performed on days 1, 4, and 7 after seeding. A metabolic assay was performed by incubation with Alamar Blue reagent (Sigma–Aldrich, 44 µM in HBSS). Cells were incubated at 37 °C for 90 min and fluorescence was measured at Ex 560 nm/ Em 590 nm.

Myofiber Characterization: After differentiation of the *C2C12* cells on the hydrogels, the formed myofibers were assessed for myoblast fusion using a desmin staining to determine the percentage of myoblasts in the cell population and a tropomyosin staining to determine the percentage of myoblasts that is able to differentiate and fuse to form myofibers. First, the hydrogel films were fixed with formaldehyde (4% PFA) for 30 min at room temperature. After fixation, the cells were rinsed three times with PBS. An additional step of permeabilization with methanol (−20 °C, 10 min) was performed. Next, blocking buffer (PBS with 0.2% Triton-X 100 and 1% bovine serum albumin, BSA, Gibco) was added to the wells with the films for 1 h to avoid non-specific binding. Anti-desmin primary antibody (Sigma, #D1033, 1:200 in blocking buffer) or anti-tropomyosin primary antibody (Sigma, #T9283, 1:100 in blocking buffer) was added and incubated overnight at 4 °C. Subsequently, the hydrogels were rinsed again three times for 5 min in PBS. Shielded from light, the hydrogels were incubated with the secondary antibody (Alexa Fluor 488, Invitrogen, 1:200 in blocking buffer, room temperature, 1 h). After additional rinsing steps (3 times 5 min with PBS), the wells were incubated with DAPI (Life Technologies, 0.1 µg mL^{-1} in PBS, room temperature, 1 h) to stain the nuclei. The samples were analyzed using a fluorescence microscope within the first 48 h to prevent fluorescence bleaching. The ratio of desmin$^+$ cells to the total amount of cells, determined by the total amount of nuclei, was calculated. Then, the fusion index (FI) was calculated as the amount of nuclei in the tropomyosin$^+$ myofibers divided by the total amount of desmin$^+$ myoblasts.[51,52] The fusion assay was calculated via an in-house ImageJ macro. Briefly, the image was split into green and blue channels, which corresponded to the immunofluorescence staining. Therefore, the green channel was used as a mask to determine the nuclei outside the tropomyosin-positive stained fibers. The nuclei which form the fibers were retrieved by the subtraction of the outside nuclei to the total.

Electromechanical Characterization: The electromechanical performance of the piezoionic GelMA has been determined using a SP-150e potentiostat (Bio-Logic Science Instruments). The samples were placed in a rectangular support structure containing two electrodes of 1 mm diameter separated by 10 mm. The electrodes were connected to the potentiostat and set in open circuit voltage measuring the potential between the two electrodes. External mechanical deformations were applied by fixing the support on the lower clamp of a tensile machine (Z2.5, ZwickRoell) while a cylindrical indenter of outer diameter 4 mm was set on the upper clamp. The output voltage amplitude and polarity as a function of the imposed compressive strains (i.e., strain rise from 1% to 50% at a constant speed of 10 mm min^{-1}) were directly recorded by the potentiostat. Since the reference electrode was placed under the indented portion, a preferential displacement of the cations over anions resulted in a positive voltage reading, and vice versa.

Ionic conductivity measurements were performed using an electrochemical impedance spectroscopy with a VSP potentiostat/galvanostat (Bio-Logic Science Instruments). Samples were placed between two gold plates of 20 mm diameter and measurements were performed with a frequency range between 1 Hz and 200 kHz by applying a 10 mV perturbation at room temperature.

Statistics: Statistical analysis was done using non-parametric one-way ANOVA test (Kruskal–Wallis) with Dunn's post-test for multiple comparisons. The mean rank of each column was compared with the mean rank of a control condition, which is the pure GelMA 0% ion condition, to guarantee an adequate statistical power of analysis. Significance level was set at 5% ($\alpha = 0.05$). A normality test was executed to verify the normal distribution of the data, before applying an ANOVA test. Triplicate measurements were obtained for each parameter reported. The analysis was performed using GraphPad Prism software (version 8.0.2). All the data were reported as the mean ± standard deviation and significance levels were indicated as $^{*}p < 0.05$, $^{**}p < 0.01$, and $^{***}p < 0.001$.

Supporting Information

Supporting Information is available from the Wiley Online Library or from the author.

Acknowledgements

This work was funded by Interreg 3D4Med, co-financed by the European Regional Development Fund, the provinces of East- and West-Flanders and the Hermes fund, and KU Leuven C24E/20/067. J.-M.R. is a senior research associate at F.R.S.-F.N.R.S. (Belgium).

Conflict of Interest

The authors declare no conflict of interest.

Author Contributions

M.B., C.G., and R.L. performed experimental design in vitro, data generation, data analysis, statistics, and data interpretation. J.V. and N.B. performed data generation, data analysis, and statistics. J.O. and J.-M.R. performed materials, data generation, data analysis, and statistics. S.V., M.G., and L.T. performed contribution of critical components and data interpretation. S.V. and L.T. performed experimental design, data interpretation, and project supervision. All authors critically contributed to writing, editing and reviewing the manuscript. The authors thank Samira Benali for administrative support.

Data Availability Statement

The data that support the findings of this study are available from the corresponding author upon reasonable request.

Keywords

biomimetic materials, gelatin, GelMA, Myoblasts, piezoionic

Received: January 19, 2023
Revised: March 23, 2023
Published online:

[1] J. M. Grasman, M. J. Zayas, R. Page, G. D. Pins, *Acta Biomater.* **2016**, *25*, 2.
[2] J. Liu, D. Saul, K. O. Böker, J. Ernst, W. Lehman, A. F. Schilling, *Biomed. Res. Int.* **2018**, *2018*, 1984879.
[3] B. E. Pollot, B. T. Corona, *Methods Mol. Biol.* **2016**, *1460*, 19.
[4] N. J. Turner, S. F. Badylak, *Cell Tissue Res.* **2012**, *347*, 759.
[5] S. Ostrovidov, V. Hosseini, S. Ahadian, T. Fujie, S. P. Parthiban, M. Ramalingam, H. Bae, H. Kaji, A. Khademhosseini, *Tissue Eng., Part B* **2014**, *20*, 403.
[6] D. W. J. Van Der Schaft, A. C. C. Van Spreeuwel, K. J. M. Boonen, M. L. P. Langelaan, C. V. C. Bouten, F. P. T. Baaijens, *J. Vis. Exp.* **2013**, *73*, e4267.
[7] H. H. Vandenburgh, *Ann. N. Y. Acad. Sci.* **2002**, *961*, 201.
[8] D. Gholobova, L. Decroix, V. Van Muylder, L. Desender, M. Gerard, G. Carpentier, H. Vandenburgh, L. Thorrez, *Tissue Eng., Part A* **2015**, *21*, 2548.
[9] D. Gholobova, M. Gerard, L. Decroix, L. Desender, N. Callewaert, P. Annaert, L. Thorrez, *Sci. Rep.* **2018**, *8*, 1.
[10] D. Gholobova, L. Terrie, K. Mackova, L. Desender, G. Carpentier, M. Gerard, L. Hympanova, J. Deprest, L. Thorrez, *Biofabrication* **2020**, *12*, 035021.
[11] P. H. U. Lee, H. H. Vandenburgh, *Tissue Eng., Part A* **2013**, *19*, 2147.
[12] L. Thorrez, K. Disano, J. Shansky, H. Vandenburgh, *Front. Physiol.* **2018**, *9*, 1076.
[13] L. Tytgat, L. Van Damme, J. Van Hoorick, H. Declercq, H. Thienpont, H. Ottevaere, P. Blondeel, P. Dubruel, S. van Vlierberghe, *Acta Biomater.* **2019**, *94*, 340.
[14] K. Yue, G. Trujillo-De Santiago, M. M. Alvarez, A. Tamayol, N. Annabi, A. Khademhosseini, *Biomaterials* **2015**, *73*, 254.
[15] J. Van Hoorick, L. Tytgat, A. Dobos, H. Ottevaere, J. Van Erps, H. Thienpont, A. Ovsianikov, P. Dubruel, S. van Vlierberghe, *Acta Biomater.* **2019**, *97*, 46.
[16] M. Zhu, Y. Wang, G. Ferracci, J. Zheng, N.-J. Cho, B. H. Lee, *Sci. Rep.* **2019**, *9*, 1.
[17] A.n I. Van Den Bulcke, B. Bogdanov, N. De Rooze, E. H. Schacht, M. Cornelissen, H. Berghmans, *Biomacromolecules* **2000**, *1*, 31.
[18] A. Ito, Y. Yamamoto, M. Sato, K. Ikeda, M. Yamamoto, H. Fujita, E. Nagamori, Y. Kawabe, M. Kamihira, *Sci. Rep.* **2014**, *4*, 1.
[19] R. D. Breukers, K. J. Gilmore, M. Kita, K. K. Wagner, M. J. Higgins, S. E. Moulton, G. M. Clark, D. L. Officer, R. M. I. Kapsa, G. G. Wallace, *J. Biomed. Mater. Res. A* **2010**, *95A*, 256.
[20] R. Dong, P. X. Ma, B. Guo, *Biomaterials* **2020**, *229*, 119584.
[21] J. Odent, T. J. Wallin, W. Pan, K. Kruemplestaedter, R. F. Shepherd, E. P. Giannelis, *Adv. Funct. Mater.* **2017**, *27*, 1701807.
[22] Y. Dobashi, D. Yao, Y. Petel, T. N. Nguyen, M. S. Sarwar, Y. Thabet, C. L. W. Ng, E. Scabeni Glitz, G. T. M. Nguyen, C. Plesse, F. Vidal, C. A. Michal, J. D. W. Madden, *Science (1979)* **2022**, *376*, 502.
[23] J. Heikenfeld, A. Jajack, J. Rogers, P. Gutruf, L. Tian, T. Pan, R. Li, M. Khine, J. Kim, J. Wang, J. Kim, *Lab Chip* **2018**, *18*, 217.
[24] T. Iwazumi, M. Noble, *Int. J. Cardiol.* **1989**, *24*, 267.
[25] A. Zaszczynska, P. Sajkiewicz, A. Gradys, *Polymers (Basel)* **2020**, *12*, 161.
[26] D.-M. Shin, S. W. Hong, Y.-H. Hwang, *Nanomaterials* **2020**, *10*, 123.
[27] C. Ribeiro, V. Sencadas, D. M. Correia, S. Lanceros-Méndez, *Colloids Surf., B* **2015**, *136*, 46.
[28] N. A. Kamel, *Biophys. Rev.* **2022**, *14*, 717.
[29] J. Odent, N. Baleine, V. Biard, Y. Dobashi, C. Vancaeyzeele, G. T. M. Nguyen, J. D. W. Madden, C. Plesse, J.-M. Raquez, *Adv. Funct. Mater.* **2022**, *33*, 2210485.
[30] A. I. van Den Bulcke, B. Bogdanov, N. De Rooze, E. H. Schacht, M. Cornelissen, H. Berghmans, *Biomacromolecules* **2000**, *1*, 31.
[31] L. Tytgat, M. Markovic, T. H. Qazi, M. Vagenende, F. Bray, J. C. Martins, C. Rolando, H. Thienpont, H. Ottevaere, A. Ovsianikov, P. Dubruel, S. Van Vlierberghe, *J. Mater. Chem. B* **2019**, *7*, 3100.
[32] K. J. M. Boonen, M. L. P. Langelaan, R. B. Polak, D. W. J. Van Der Schaft, F. P. T. Baaijens, M. J. Post, *J. Biomech.* **2010**, *43*, 1514.
[33] M. L. P. Langelaan, K. J. M. Boonen, K. Y. Rosaria-Chak, D. W. J. van derSchaft, M. J. Post, F. P. T. Baaijens, *Ann. Am. Thorac. Soc.* **2010**, *12*, 181.
[34] Y. Wu, Y. X. Chen, J. Yan, D. Quinn, P. Dong, S. W. Sawyer, P. Soman, *Acta Biomater.* **2016**, *33*, 122.
[35] S. W. Sawyer, P. Dong, S. Venn, A. Ramos, D. Quinn, J. A. Horton, P. Soman, *Biomed. Phys. Eng. Express* **2018**, *4*,015005.
[36] I. Van Nieuwenhove, A. Salamon, K. Peters, G.-J. Graulus, J. C. Martins, D. Frankel, K. Kersemans, F. De Vos, S. Van Vlierberghe, P. Dubruel, *Carbohydr. Polym.* **2016**, *152*, 129.
[37] R. Luo, H. Li, *Acta Biomater.* **2009**, *5*, 2920.
[38] P. Li, N. H. Kim, D. Hui, K. Y. Rhee, J. H. Lee, *Appl. Clay Sci.* **2009**, *46*, 414.
[39] F. Tan, X. Xu, T. Deng, M. Yin, X. Zhang, J. Wang, *Biomed. Mater.* **2012**, *7*,055009.
[40] Q. Xing, K. Yates, C. Vogt, Z. Qian, M. C. Frost, F. Zhao, *Sci. Rep.* **2014**, *4*, 4706.
[41] G.-J. Graulus, A. Mignon, S. Van Vlierberghe, H. Declercq, K. Fehér, M. Cornelissen, J. C. Martins, P. Dubruel, *Eur. Polym. J.* **2015**, *72*, 494.
[42] J. Van Hoorick, P. Gruber, M. Markovic, M. Tromayer, J. Van Erps, H. Thienpont, R. Liska, A. Ovsianikov, P. Dubruel, S. Van Vlierberghe, *Biomacromolecules* **2017**, *18*, 3260.
[43] J. Van Hoorick, H. Declercq, A. De Muynck, A. Houben, L. Van Hoorebeke, R. Cornelissen, J. Van Erps, H. Thienpont, P. Dubruel, S. Van Vlierberghe, *J. Mater. Sci.: Mater. Med.* **2015**, *26*, 247.
[44] S. Van Vlierberghe, B. Fritzinger, J. C. Martins, P. Dubruel, *Appl. Spectrosc.* **2010**, *64*, 1176.
[45] N. Rajabi, M. Kharaziha, R. Emadi, A. Zarrabi, H. Mokhtari, S. Salehi, *J. Colloid Interface Sci.* **2020**, *564*, 155.
[46] Q. Huang, Y. Zou, M. C. Arno, S. Chen, T. Wang, J. Gao, A. P. Dove, J. Du, *Chem. Soc. Rev.* **2017**, *46*, 6255.
[47] X. Chen, W. Du, Z. Cai, S. Ji, M. Dwivedi, J. Chen, G. Zhao, J. Chu, *ACS Appl. Mater. Interfaces* **2020**, *12*, 2162.
[48] W. Kim, H. Lee, J. Lee, A. Atala, J. J. Yoo, S. J. Lee, G. H. Kim, *Biomaterials* **2020**, *230*, 119632.
[49] L. Tytgat, L. Van Damme, J. Van Hoorick, H. Declercq, H. Thienpont, H. Ottevaere, P. Blondeel, P. Dubruel, S. Van Vlierberghe, *Acta Biomater.* **2019**, *94*, 340.
[50] N. Atale, S. Gupta, U. C. S. Yadav, V. Rani, *J. Microsc.* **2014**, *255*, 7.
[51] P. Bajaj, B. Reddy, L. Millet, C. Wei, P. Zorlutuna, G. Bao, R. Bashir, *Integr. Biol.* **2011**, *3*, 897.
[52] R. Mccoll, M. Nkosi, C. Snyman, C. Niesler, *BioTechniques* **2016**, *61*, 323.

